

## Full length article

## Experimental, numerical, and analytical studies of asymmetric bolted square hollow section splices in bending

Rui Yan<sup>a,b,\*</sup>, Milan Veljkovic<sup>a</sup>, Luís Simões Da Silva<sup>c</sup><sup>a</sup> Department of Engineering Structures, Delft University of Technology, Delft, the Netherlands<sup>b</sup> Department of Civil and Environmental Engineering, The Hong Kong Polytechnic University, Hong Kong, PR China<sup>c</sup> Department of Civil Engineering, ISE, ARISE, University of Coimbra, Coimbra, Portugal

## ARTICLE INFO

## Keywords:

Component method  
Asymmetric tubular splices  
Bolted connection  
Square hollow section

## ABSTRACT

The flexural behaviour of two types of asymmetric bolted square hollow section (SHS) splices is investigated in this paper. The asymmetric bolted SHS splices are derived from the traditional bolted end plate SHS joints but with the end plate flushed to the SHS surface on one side or two adjacent sides, where a cover plate connects two SHSs. Firstly, four-point bending tests are conducted for two configurations under different loading conditions. Next, finite element (FE) analysis is carried out to simulate the experiments. To reduce the computational time, a simplified FE model is developed, which is further employed for a parametric study. Finally, the component method, which was extended for the asymmetric bolted SHS splices under tensile load, is verified against the FE models in the parametric study. The results show that the extended component method could effectively predict the stiffness and the resistance of bolted asymmetric SHS splices under different bending loads.

## 1. Introduction

Bolted connections and welded connections are two main technologies for connections in steel structures, e.g., column bases, beam-to-column joints, beam splices, and column splices. The construction cost, in terms of price and time, may be reduced using off-site prefabricated structures, where the structure members are prefabricated in workshops and assembled on-site. Significant research has been conducted on bolted connections from different perspectives, such as the mechanical behaviour of innovative joints [1–5], design models for bolted connections [6–10], and steel-to-concrete connections [11,12].

Hollow sections are typical structural profiles with light self-weight, excellent torsional resistance, and a visually attractive appearance. Different types of bolted connections [13–20] have been proposed for hollow sections, which provide alternative solutions for traditional joints and splices to enable quick and simple assembly. For example, the traditional solution for square hollow section (SHS) column splices is to connect two members by end plates. Kato and Mukai [21] propose a two-dimensional yield line model to design the tensile resistance of SHS splices with bolts on four sides. For the rectangular hollow section (RHS) splices with bolts on two opposite sides, a one-dimensional design model with six failure modes is proposed by Packer et al. [22]. The design

models are based on the assumption of the plastic hinge on the end plate, represented by the yield lines. The length of the yield line is essential for calculating the resistance of the connection. Steige and Weynand [23] propose an equation to calculate the effective length of the yield line at the corner of the end plate, based on a two-dimensional yield line model for RHS splices developed by Willibald [24]. For the RHS splices with bolts only at four corners, Heinisuo et al. [25] define three failure modes with different yield line patterns. Regarding the stiffness of the RHS splices, Karlsen and Aalberg [26] find that the existing T-stub model, which is used in FprEN 1993-1-8 [27] for open cross-sections, is not suitable for RHS splices. A new stiffness model is proposed considering the effect of the two-dimensional bending interaction of the end plate inside the tube.

The traditional configurations require an installation gap between the column surface and the façade panel for columns at the outer corner or along the façade of a building. To address this issue, two new asymmetric configurations, as shown in Fig. 1, were proposed for the column splices at the corner (Corner column splice, CCS) and along the façade (Wall column splice, WCS) [2].

The proposed splices consist of cold-formed SHS tubes, end plates, cover plates, M24 bolts for connecting end plates, and M20 bolts for connecting cover plates. The end plate is welded to SHS1 and SHS2 on

\* Corresponding author.

E-mail address: [cee-rui.yan@polyu.edu.hk](mailto:cee-rui.yan@polyu.edu.hk) (R. Yan).<https://doi.org/10.1016/j.tws.2024.112282>

Received 15 March 2024; Received in revised form 20 July 2024; Accepted 27 July 2024

Available online 30 July 2024

0263-8231/© 2024 The Author(s). Published by Elsevier Ltd. This is an open access article under the CC BY license (<http://creativecommons.org/licenses/by/4.0/>).

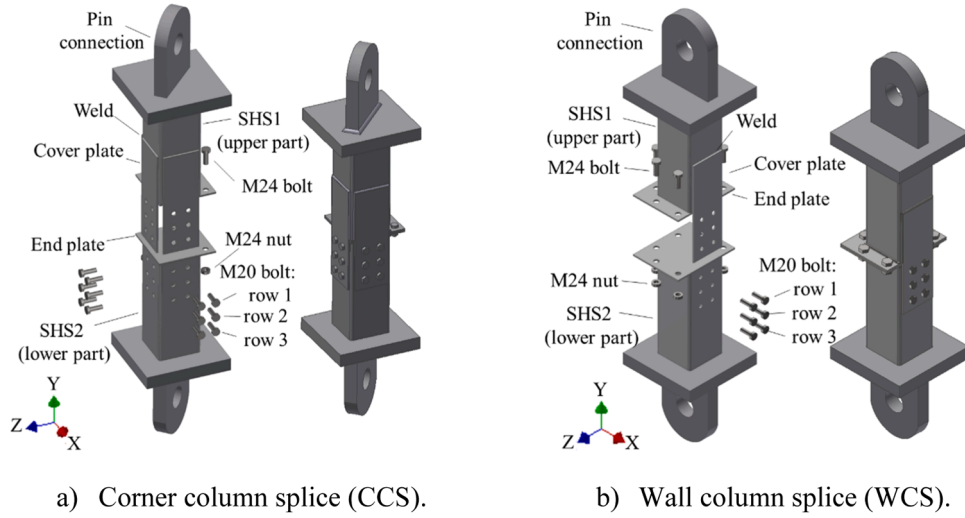


Fig. 1. Two new configurations of asymmetric column splices. [2].

Table 1

Thickness of plates and welds [mm].

Configuration	NO.	Measured weld	FE weld	End plate	Cover plate	SHS
WCS-CPT-6	A	7.6	7.5	6.0	6.0	7.7
	B	7.3				
WCS-CPC-6	A	7.5	7.5			
	B	8.0				
WCS-CPB-6	A	7.2	7.5			
	B	7.3				
CCS-CPT-6	A	8.7	9.1			
	B	9.4				
CCS-CPC-6	A	9.2	9.1			
	B	8.9				
WCS-CPT-8	A	8.5	8.7	8.5	7.9	
	B	9.0				
WCS-CPC-8	A	8.5	8.7			
	B	8.9				
WCS-CPB-8	A	9.3	9.4			
	B	9.4				
CCS-CPT-8	A	9.0	9.0			
	B	9.2				
CCS-CPC-8	A	8.9	9.0			
	B	9.0				

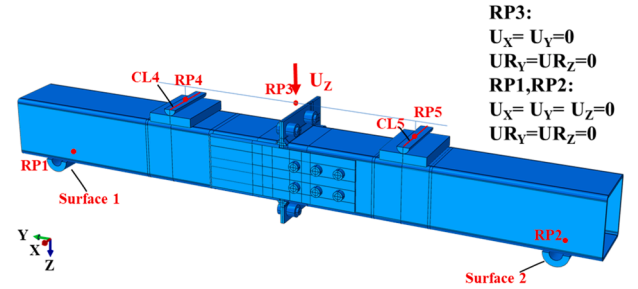


Fig. 3. Finite element model.

This paper, which is a continuation of the previous two studies [2,10], presents the experimental, numerical, and analytical studies on the bending behaviour of asymmetric splices. The extended component method is used to predict the resistance and stiffness of two types of asymmetric bolted SHS splices under different types of bending load.

## 2. Experiments and finite element (FE) analysis

### 2.1. Specimens and test setup

Considering the asymmetric feature of the splices, five loading conditions are characterised for the two configurations, as follows: WCS with cover plate in tension (WCS-CPT), WCS with cover plate in compression (WCS-CPC), WCS with cover plate in bending (WCS-CPB), CCS with cover plate in tension (CCS-CPT), and CCS with cover plate in compression (CCS-CPC). Two nominal thicknesses (6 mm and 8 mm) of the end plate and the cover plate are tested in the experiments. The column of the tested specimens is  $200 \times 200 \times 8$  square hollow section (SHS). Both M24 and M20 bolts are grade 10.9 hexagonal head bolts. Note that the M20 bolts should be replaced by blind bolts in real structures. It is worth mentioning that replacing the blind bolt with the normal bolt results in a limited difference in resistance, while the stiffness might deviate slightly depending on the type of the blind bolt. Swierczyna [28] compares the initial stiffness of lap joints using the normal bolt and the blind bolts with a sleeve. It is found that using the blind bolt leads to a relatively high initial stiffness, resulting from the lack of slip in the blind bolt joint where the fastener sleeve tightly fills the bolt hole during installation. It is also argued that the difference would be smaller if the tolerance of the bolt hole is 1 mm. In addition, for the blind bolt without a sleeve and requiring standard bolt hole

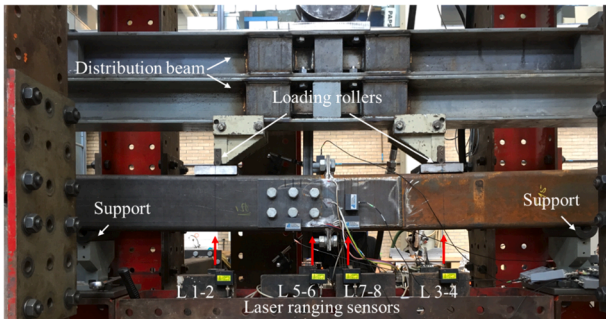


Fig. 2. Experimental setup.

the sides without the cover plate. The cover plate is welded to the SHS1 on three sides around the cover plate. Under the framework of the component method in FprEN 1993-1-8 [27], the behaviour of the individual components and the interaction between different components are studied by Yan et al. [10]. The proposed component method can accurately predict the tensile behaviour of the two asymmetric splices.

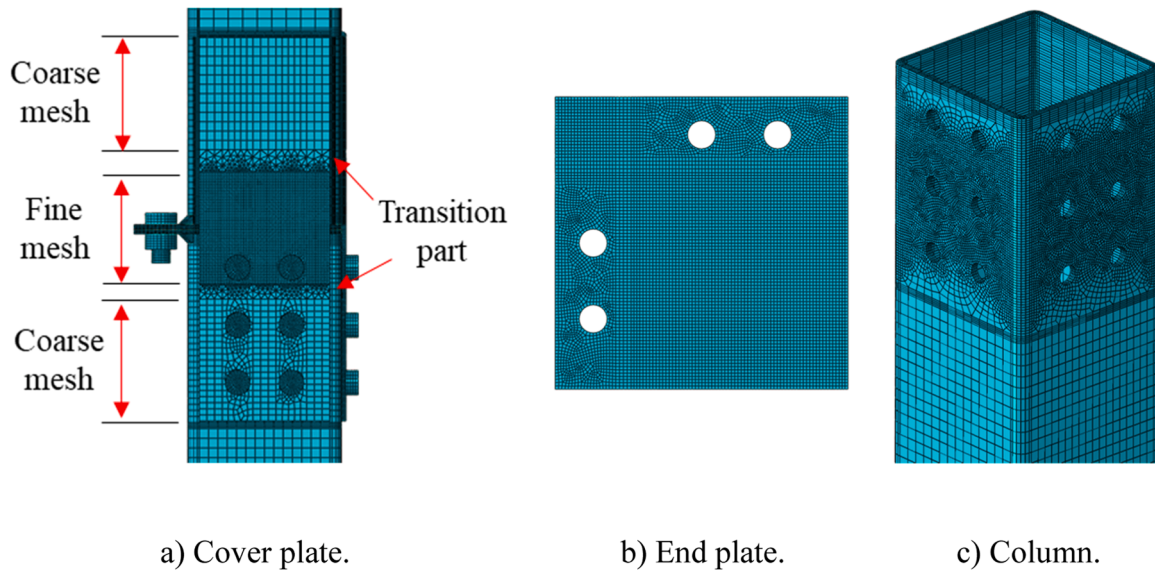


Fig. 4. Mesh details. [2].

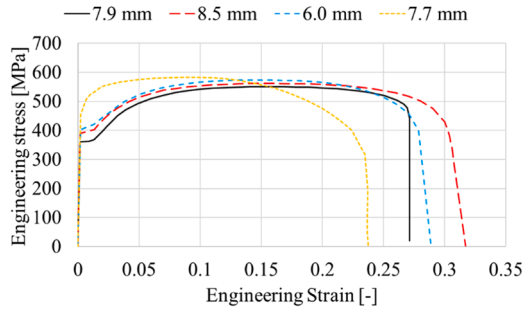


Fig. 5. Engineering stress-strain relationships. [2].

**Table 2**  
Material properties of plates. [2].

Thickness [mm]	$E$ [GPa]	$f_y$ [MPa]	$\epsilon_y$ [%]	$f_u$ [MPa]	$\epsilon_u$ [%]	$f_u/f_y$	$\epsilon_f$ [%]
6.0	193	404	0.209	574	14.07	1.42	28.9
7.7	194	479	0.447	583	8.56	1.28	23.7
7.9	197	361	0.183	551	16.11	1.53	27.1
8.5	200	391	0.196	562	14.08	1.44	30.8

tolerance [29], the stiffness difference compared to the normal bolt should be very limited. Hence, the component method presented in this paper also suits the joint using blind bolts with 1 mm bolt hole tolerance and blind bolts without a sleeve.

The nominal dimensions of the splices are shown in Appendix A. The measured thicknesses of the plate, SHS, and the throat thickness of the weld on the end plate are presented in Table 1, where the last number of the specimen name is the plate nominal thickness. Each test was performed in two repetitions, resulting in 20 tests in total. Note that the tested splices are intentionally designed weaker than the column because the study aims to develop and verify the component method for the involved components. Hence, the failure of the specimen was governed by the investigated components. In real applications, the joint is often designed to be stronger than the column, especially for structures with the seismic design. The present study provides a solution to evaluate the resistance of the joint. A joint stronger than the column can be designed using the proposed method, while the possibility of designing a

more economical joint, where the bending failure is not critical, e.g., the column which is dominated by compression load, remains.

A four-point bending setup is used to test all specimens, as shown in Fig. 2. A distribution beam, which is pinned to the jack, is used to ensure the same load at two loading points. The load is spread from rollers to the specimen in a broader range through two thick plates to avoid potential local buckling failure of the tube. The specimens are simply supported at two ends of the specimen (with a 1730 mm distance) and loaded by a pair of round rollers. The distances between the two rollers are 700 mm and 800 mm for specimens with 8 mm and 6 mm plates, respectively. All tests are executed in displacement control with a constant loading rate of 0.012 mm/s.

Eight or six laser ranging sensors are employed to measure the vertical displacements of specimens with the end plate or the cover plate at the bottom side during testing, respectively. Two pairs of lasers (L1–2 and L3–4) are positioned at the loading cross-sections. For specimens with an end plate at the bottom, two pairs of lasers (L5–6 and L7–8) measure the deformation of the cross-sections of the plate with a 50 mm distance to the surface of the end plate, as shown in Fig. 2. For the specimen with a cover plate at the bottom, one pair of lasers (L5–6) are pointed on the cover plate at the cross-section where two end plates meet.

## 2.2. Finite element (FE) models

The commercial software ABAQUS 6.14 [30] is used to simulate the four-point bending tests. Fig. 3 depicts the details of the FE model. A distribution beam is created using a B31 linear beam element to reduce the number of elements and save computational time. The load is applied via a vertical displacement at Reference Point 3 (RP3) which is at the middle point of the distribution beam. Two reference points on the distribution beam, RP4 and RP5, are connected to the corresponding Central Lines 4 and 5 (CL4 and CL5) in the half-circular rollers. CL4 and CL5 could freely rotate around the X axis while the corresponding reference point constrains the rest degrees of freedom. The bottom surfaces of the support roller (Surface 1 and Surface 2) are slaved by RP1 and RP2 in all six degrees of freedom, respectively. The detailed boundary conditions of RP1, RP2, and RP3 are given in Fig. 3. The property of contact pairs was set as the hard contact in the normal direction and penalty friction with the friction coefficient of 0.2 for the tangential behaviour.

The mesh sensitivity is evaluated in the companion study [2], where the tensile behaviour of the asymmetric joints is investigated. It is concluded that a 3 mm mesh size is sufficient to predict the mechanical

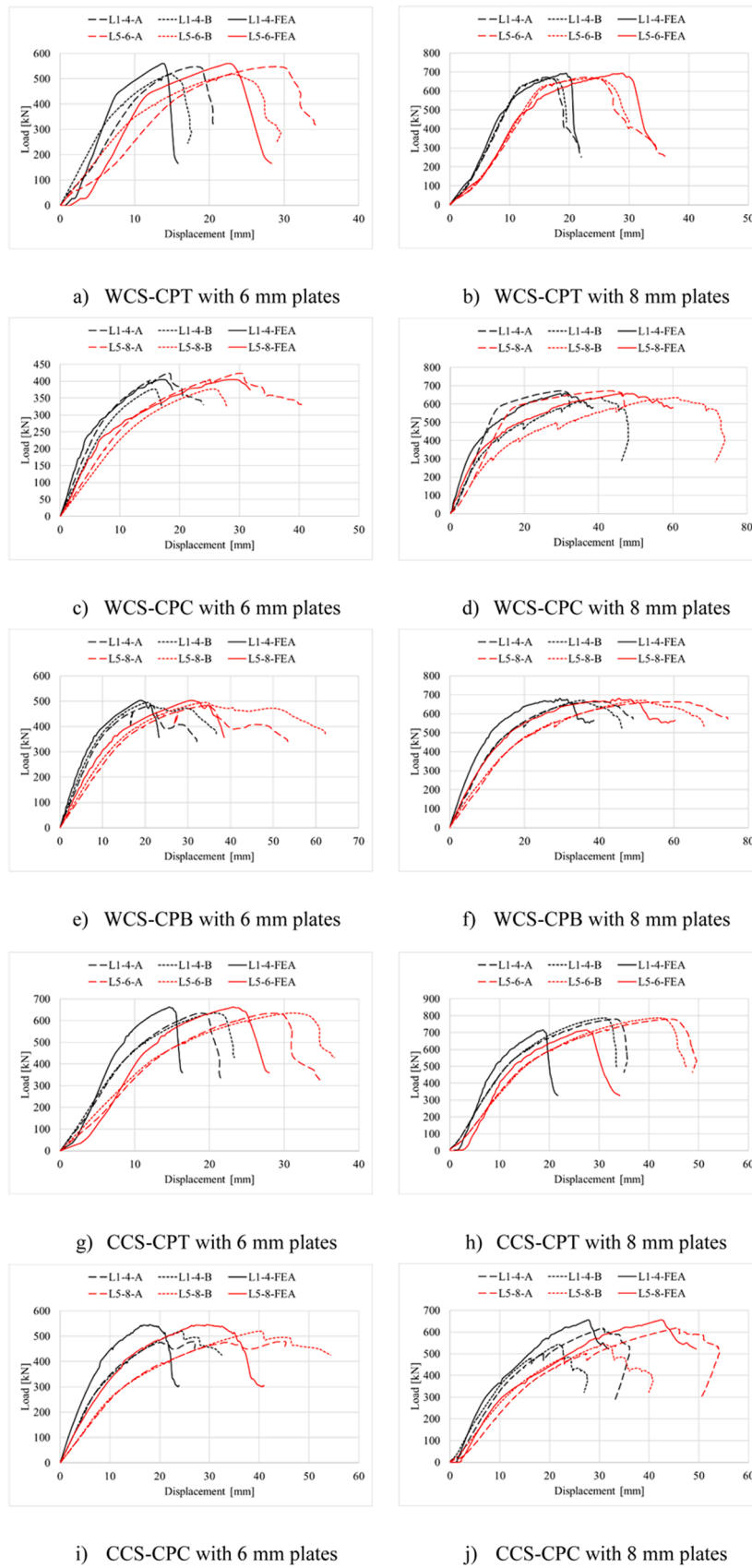


Fig. 6. Comparison of load-displacement relationships.



**Table 3**

Comparison of the maximum resistance [kN].

Load case	NO.	6mm			8mm		
		EXP	FEA	ERR[%]	EXP	FEA	ERR[%]
WCS-CPT	A	548	562	2.5	673	693	3.0
	B	518		8.4	665		4.2
WCS-CPC	A	424	404	-4.6	672	657	-2.3
	B	377		7.2	635		3.5
WCS-CPB	A	483	502	4.1	663	712	2.6
	B	495		1.6	670		1.5
CCS-CPT	A	634	662	4.3	780	715	-8.4
	B	635		4.2	787		-9.2
CCS-CPC	A	479	545	13.9	619	654	5.7
	B	520		5.0	543		20.4

where ERR is  $(FEA/EXP-1) \times 100$ .

behaviour of the critical region. In this study, a 3 mm mesh size is used in the potential fracture region, and the mesh size is gradually increased to 9 mm elsewhere. The mesh is the same as in [2], see Fig. 4.

### 2.3. Material mechanical properties

The mechanical properties of different materials obtained from tensile coupon tests are employed in the FE models. The engineering stress-strain relationships for each thickness of the material are plotted in Fig. 5, and the characterised mechanical properties are summarised in Table 2, where  $E$ ,  $f_y$ ,  $\epsilon_y$ ,  $f_u$ ,  $\epsilon_u$ , and  $\epsilon_f$  are the measured Young's modulus, yield strength, yield strain, ultimate strength, ultimate strain, and fracture at elongation, respectively. Note that  $\epsilon_y$  is calculated by  $f_y/E$  for plates (6 mm, 7.9 mm, and 8.5 mm) with yield plateau. For the 7.7 mm plate without a yield plateau,  $\epsilon_y$  equals  $0.002 + f_y/E$ . Fracture is not observed in the weld in all specimens. Hence, the weld is not critical for the joint. The same material model is assumed for the end plate and the weld. The throat thickness of the weld is presented in Table 1. Mises yield criterion is employed in the FE analysis.

### 2.4. Validation of FE models

The FE models are validated against the experiments in terms of load-deformation relationships and failure modes. Fig. 6 compares the load-deformation relationships of each type of specimen. Since the laser sensors are symmetrically positioned around the interface of two end plates, the measured deformations at symmetric positions are averaged, i.e., L1-L4 at loading points are averaged as L1-4. The letters A and B represent the two repetitions, and FEA is the result of the FE model. Table 3 shows that FEMs could well predict the ultimate resistance with a 6 % average deviation. The resistance of CCS-CPC-8-B is significantly lower than the FE prediction due to the fabrication deficiency. The typical failure mode of CCS-CPC is a fracture in the side cover plate and fracture cutting through the end plate, as shown in Fig. 6. However, fracture occurred beneath the weld on the end plate but not in the cover plate in specimen CCS-CPC-8-B, indicating that the weak heat-affected zone (HAZ) results in premature failure. The weld thickness at the corner of the SHS near the cover plate side is very small, and the welding process resulted in a weak HAZ. Due to the tolerance of the bolt hole, the small gap between two end plates, and the representativeness of the measured size of the fillet weld, the stiffness of the FEM is slightly higher than the experimental results in some cases.

PEEQ contour plots of FE models are compared to the most representative failure modes for each configuration under different loading conditions in Fig. 7. Two typical failure modes can be identified from the experiments, including the fracture at the net section of the cover plate and the fracture at the toe of the weld in the end plate. Fig. 7 demonstrates that high PEEQ appears at the position where the fracture occurs in experiments, indicating that FE models could successfully predict the failure modes.

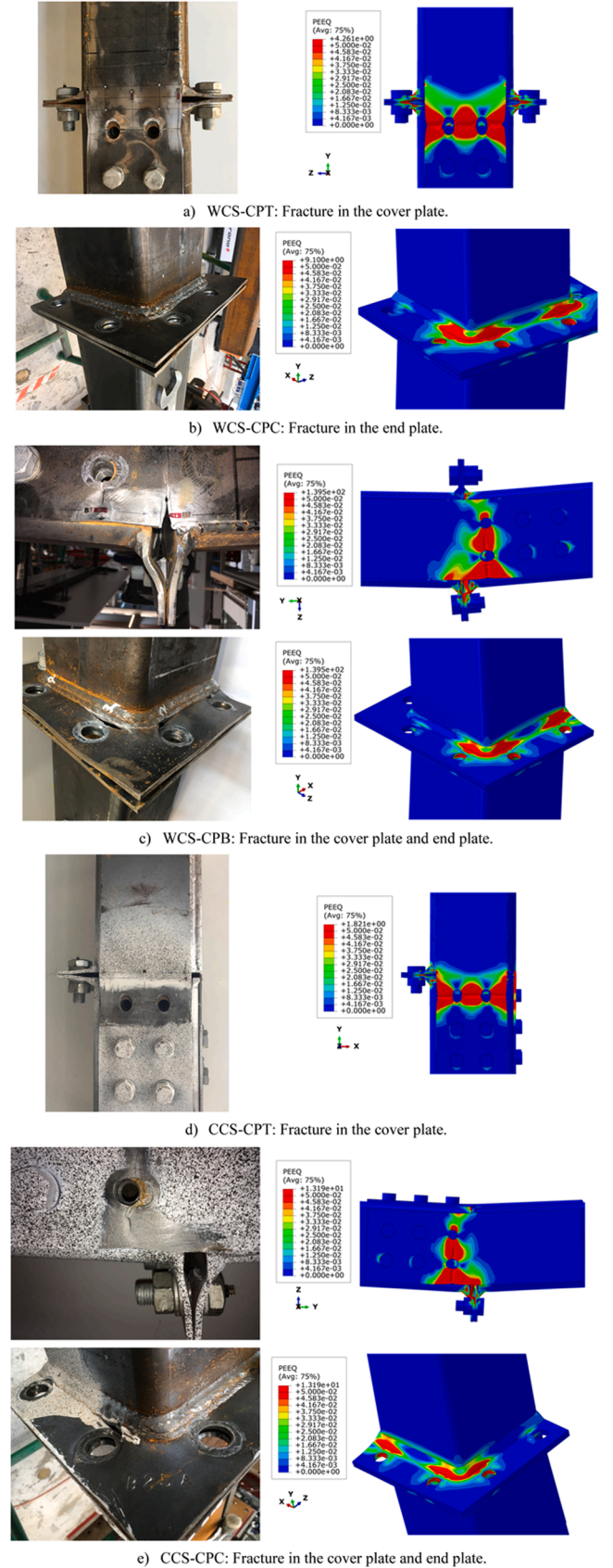


Fig. 7. Comparison of experimental and FE failure modes.

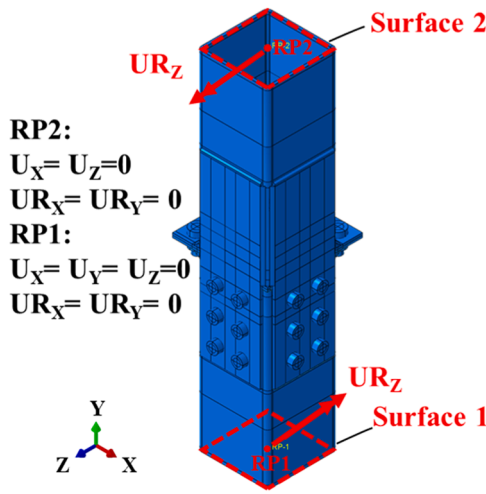


Fig. 8. Simplified FE model (CCS-CPT).

### 2.5. Simplified FE models

It is quite time-consuming to conduct a parametric study using the validated four-point bending FE model, considering the complicated contacting surfaces in the load and support rollers and the large number of elements. Hence, a simplified FE model is generated based on the four-point bending model. The length of the column is reduced from 1000 mm to 500 mm. The load is modified from the vertical displacement of the roller to a rotation angle at the end cross-section (surface) of the column, as shown in Fig. 8. Two reference points (RP1 and RP2) are created at the centre of the top and bottom cross-sections (surfaces), Surface 1 and Surface 2. Surface 1 and Surface 2 are constrained by RP1 and RP2 via the Rigid Body constraint. All degrees of freedom at RP1 are constrained except for the rotation around the Z axis. All degrees of freedom at RP2 are constrained except for the rotation around the Z axis and the displacement in the Y direction. The same magnitude of cross-section rotation deformation is applied to RP1 and RP2 but in the opposite direction. Fig. 8 depicts an example of a corner splice under the load case of the cover plate in tension (CCS-CPT).

The moment-rotation relationships of the simplified models are compared to that of all the four-point bending models. In the four-point bending model, the rotation angle of the splice is calculated based on the horizontal displacement (Y direction in Fig. 3) of the elements at the loading cross-sections. The moment is a half of the total load times the lever arm. In the simplified model, the moment and rotation angle could be directly extracted from two reference points RP1 and RP2. The comparison is made for all ten types of tests. Good agreements are observed between the two models. Due to the page limit, the results of WCS with 6 mm plates are presented in Fig. 9. Hence, the simplified models are validated and used further in the parametric study.

### 2.6. Parametric study

The nominal material properties for S355 according to prEN 1993-1-1 [31] and for the grade 10.9 bolt according to FprEN 1993-1-8 [27] are employed in the parametric study. The Young's modulus ( $E$ ) of both materials is 200 GPa. The engineering stress-strain relationships are shown in Fig. 10.

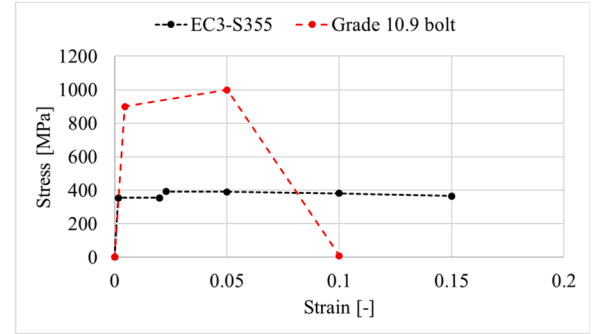


Fig. 10. Stress-strain relationships.

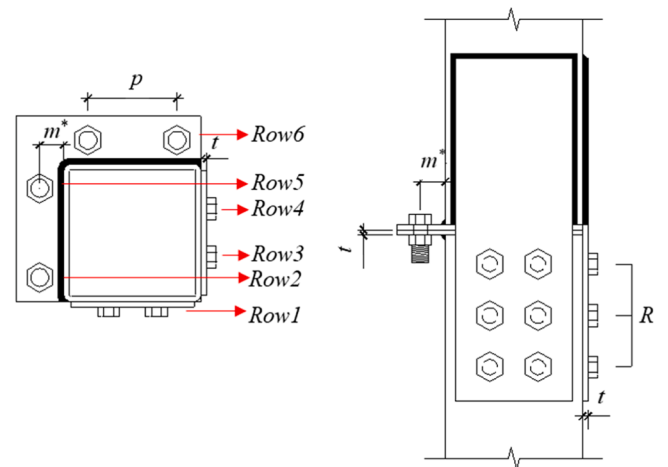


Fig. 11. Parameters used in the analysis.

Table 4

Range of investigated parameters.

Parameters	Dimensions		
$m^*$ [mm]	35	50	65
$t$ [mm]	6	8	10
$p$ [mm]	130	100	70
$R$	3	2	1

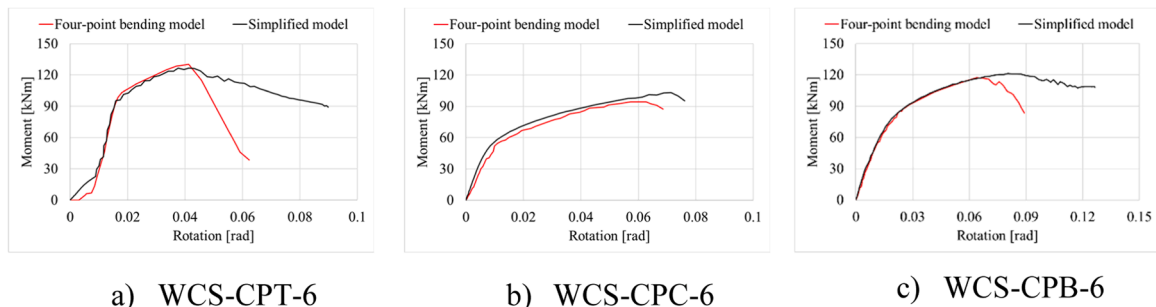
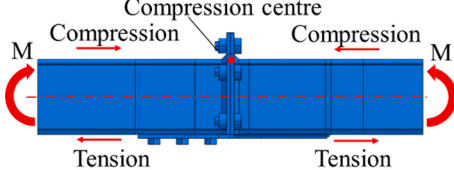
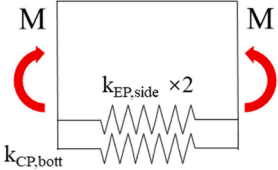
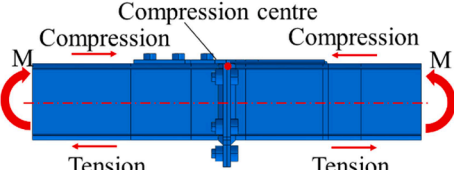
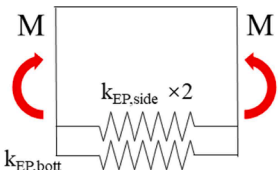
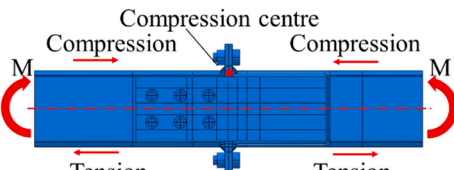
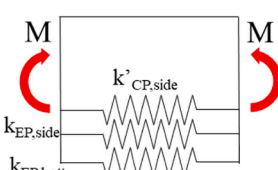
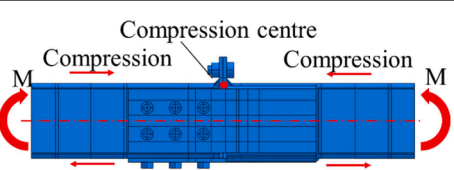
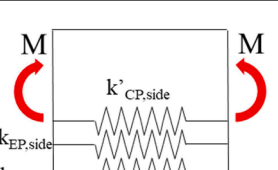
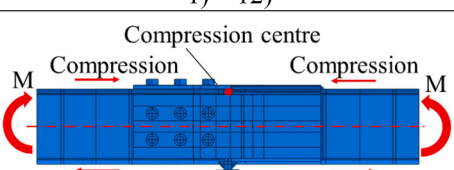
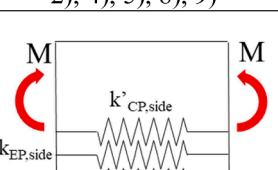


Fig. 9. Comparison of the four-point bending model and the simplified model.

**Table 5**  
Active components for various load cases of asymmetric splices.

Load case	Resistance model	Stiffness model
WCS-CPT		
	1) – 12)	2), 4), 5), 8), 9)
WCS-CPC		
	8) – 10), 12)	8), 9)
WCS-CPB		
	1) – 12)	2), 4), 5), 8), 9)
CCS-CPT		
	1) – 12)	2), 4), 5), 8), 9)
CCS-CPC		
	1) – 12)	2), 4), 5), 8), 9)

Four parameters are investigated in this study: the thickness of the end plate and the cover plate ( $t$ ), the distance from the tube outside wall to the centre of the bolt hole ( $m^*$ ), the bolt pitch on the end plate ( $p$ ), and the number of bolt rows on the cover plate ( $R$ ). The meaning of each parameter is depicted in Fig. 11. The range of each parameter is listed in Table 4.

### 3. Component method

The component method is used to predict the resistance and stiffness of bolted joints based on the behaviour of individual components, as stipulated in FprEN 1993-1-8 [27]. The following 12 components are identified in the five load cases investigated:

- Seven components are related to the cover plate:
  - 1) Plate in tension (cover plate)

- 2) Bolts in bearing (cover plate)
- 3) Block tearing failure of the cover plate
- 4) Bolts in shear
- 5) Bolts in bearing (column)
- 6) Block tearing failure of the column
- 7) Welds (cover plate)
  - Three components are related to the end plate:
    - 8) End plate in bending
    - 9) Bolts in tension
    - 10) Welds (end plate)
  - Two components are related to the column:
    - 11) Plate in tension (column)
    - 12) Column flange and web in compression

The active components in each load case are summarised in Table 5. The design formulas for 11 components are available in FprEN 1993-1-8

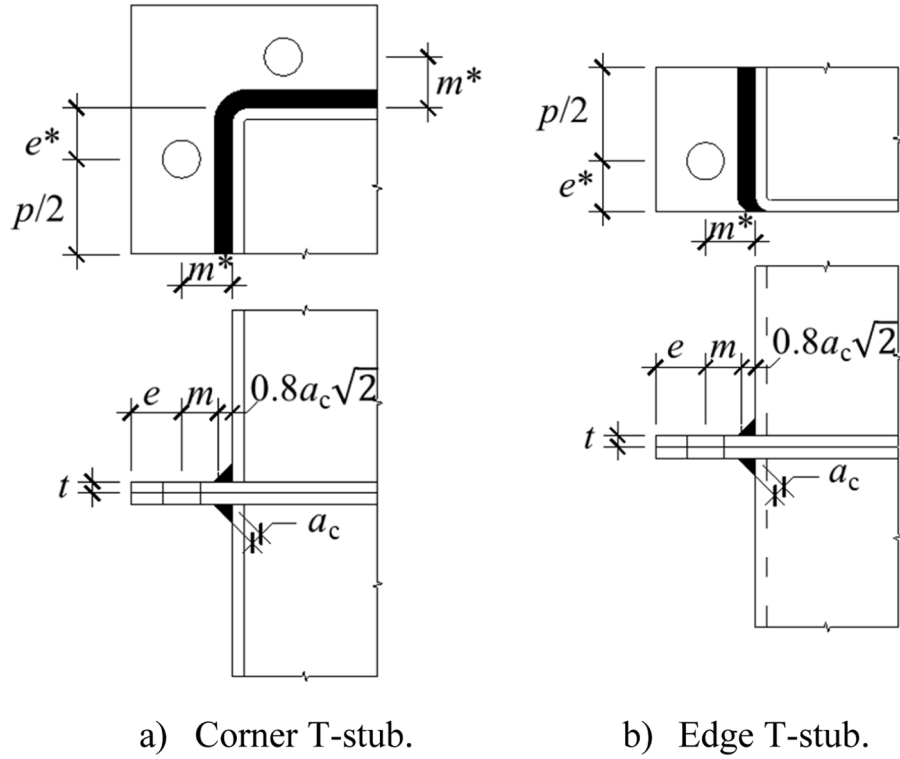


Fig. 12. Two types of T-stubs [10].

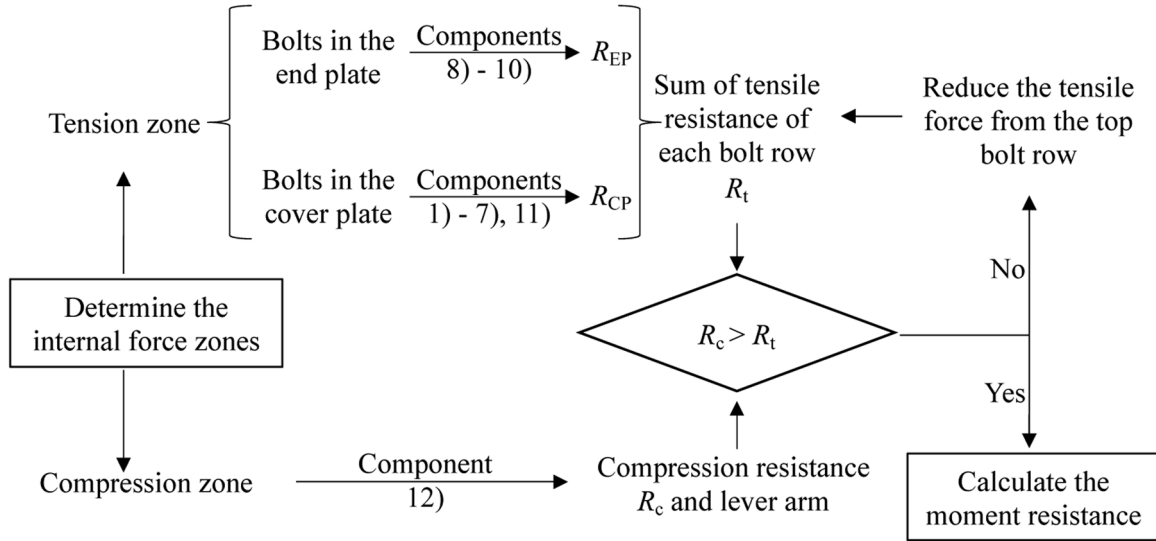


Fig. 13. Flow chart for the resistance calculation.

[27]. The Component 8) – end plate in bending with a hollow section is derived in [10] for two types of T-stubs shown in Fig. 12. The Corner T-stub (CT) and the Edge T-stub (ET) are suitable for the bolted end plate connection with bolts on four sides and two sides of the square hollow section, respectively. The proposed prediction model in [10] was successfully validated against experiments of the two asymmetric splices loaded in tension. In the present study, the prediction models for CT and ET are adopted for the T-stub away from and adjacent to the cover plate, respectively. The design formulas for the resistance and stiffness calculations are presented in Appendix B and Appendix C, respectively.

### 3.1. Resistance prediction results

The basic concept of the component method is to sum up the moment resistances of each bolt row, e.g., the tensile resistance multiply the corresponding lever arm. The compression force is transferred directly through the top wall of the tubular profile, referring to figures in Table 5. Hence, the lever arm for each bolt row is determined as the distance from the bolt row to the compression centre, indicated by a red point in Table 5. As bolt rows close to the compression centre have limited contribution to the moment resistance, only bolt rows below the centroid of the column (red dash-dot line) are considered in the calculation.

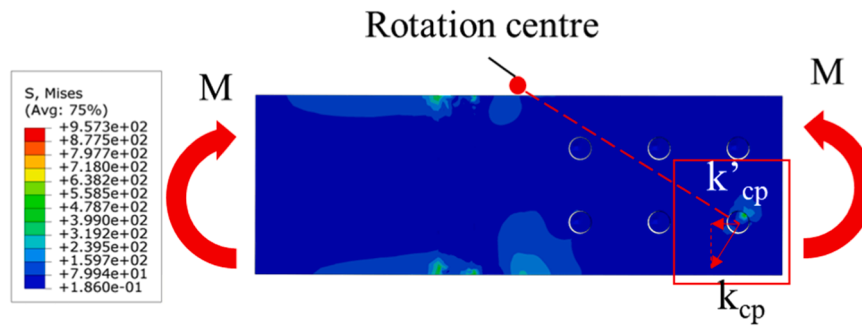
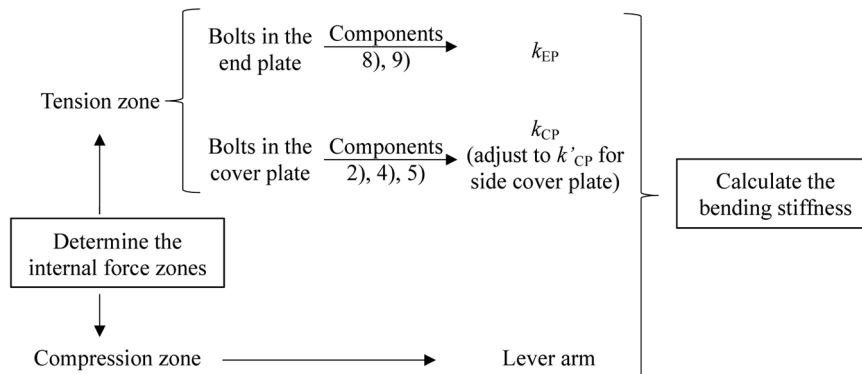
Take CCS-CPT presented in Table 5, for instance. Bolt rows 1, 2, and



**Table 6**

Resistance predictions [kNm].

	WCS-CPT			WCS-CPC			WCS-CPB			CCS-CPT			CCS-CPC		
	CM	FE	ERR [%]	CM	FE	ERR [%]	CM	FE	ERR [%]	CM	FE	ERR [%]	CM	FE	ERR [%]
t6RM	92	95	-3	62	66	-5	71	66	7	103	104	-1	70	67	5
t8RM	124	129	-4	91	99	-8	100	105	-4	134	132	2	100	101	-1
t6m35	68	73	-8	55	60	-9	57	60	-4	73	72	1	57	56	3
t6m50	61	60	2	43	40	7	48	54	-11	70	66	5	48	53	-9
t6m65	56	54	4	26	29	-11	36	43	-17	67	66	2	36	42	-16
t6P70	64	70	-8	48	60	-20	54	55	-2	71	73	-2	56	52	6
t6P100	66	73	-9	52	60	-14	56	59	-4	72	74	-3	57	58	-2
t8P70	90	93	-4	76	86	-11	83	97	-15	97	94	3	83	88	-5
t8P100	94	96	-3	82	91	-9	86	96	-11	99	96	3	87	88	-1
t6	68	73	-8	55	60	-8	57	59	-2	73	73	1	57	56	3
t8	95	98	-3	83	88	-6	85	94	-10	99	96	4	85	88	-3
t10	114	117	-2	101	102	-1	103	109	-5	120	115	4	103	111	-7
t12	124	125	-1	128	122	4	123	124	-1	125	120	4	123	128	-4
t8R2	68	74	-9	55	60	-8	57	54	7	73	68	7	57	51	13
t8R1	54	63	-14	55	60	-8	53	47	13	55	52	6	53	45	18
t6R2	95	100	-5	83	88	-6	85	80	6	99	92	8	85	77	11
t6R1	69	75	-9	83	88	-6	77	73	5	64	59	9	77	69	10

**Fig. 14.** Number of activated bolts in the cover plate in bending.**Fig. 15.** Flow chart for the stiffness calculation.

3 (see Fig. 11) are considered in the resistance calculation. The bolt rows 1 and 3 refer to Components 1) – 7) and 11). The bolt row 2 refers to Components 8) – 10), where the model for ET should be used. In the case of CCS-CPC, bolt rows 4, 5, and 6 are assumed active. The difference compared to CCS-CPT is that bolt row 5 uses the CT model while bolt row 6 employs both CT and ET models. Fig. 13 shows a flow chart of the resistance calculation steps.

The predicted resistances of the FE parametric study are summarised in Table 6. The resistance of the FE model (symbol FE) is determined based on the stress level of the component in the tension zone. For WCS-CPT and CCS-CPT where a cover plate is loaded in tension, the moment resistance is determined when the resultant force in the cover plate,

extracted from the FE results, reaches the designed resistance on the cover plate side based on Components 1) – 7) and 11). For WCS-CPC, CCS-CPC, and CCS-CPB with an end plate connection loaded in tension, the determined resistance corresponds to the stage when 5 % equivalent plastic strain (PEEQ) is reached in the end plate. These two criteria are the same as those in [10] where the design model is derived.

Regarding the failure modes obtained in the parametric study, in addition to the failure mode in Fig. 6, high plastic strain concentration at the net cross-section of the column is observed in models using 12 mm plates. The failure mode of the FE model is not presented, as high strain concentration can be observed at different parts of the model, which makes the exact failure mode difficult to distinguish using our FE model.

**Table 7**  
Stiffness prediction [kNm/rad].

	WCS-CPT			WCS-CPC			WCS-CPB			CCS-CPT			CCS-CPC		
	CM	FE	ERR	CM	FE	ERR	CM	FE	ERR	CM	FE	ERR	CM	FE	ERR
t6RM	14	13	7	9	8	17	7	6	16	14	14	2	7	6	8
t8RM	16	13	20	12	11	11	10	8	17	17	17	-2	10	9	11
t6m35	13	12	6	9	9	5	7	7	6	11	11	-2	7	7	4
t6m50	11	11	-3	4	4	-6	3	3	-3	10	10	2	3	3	-5
t6m65	10	10	5	2	2	-7	2	2	4	10	10	-2	1	1	-1
t6P70	11	11	6	6	6	0	6	5	6	11	11	1	6	5	16
t6P100	12	12	2	8	8	0	6	6	4	11	11	3	7	6	13
t8P70	14	12	12	9	8	7	8	7	14	12	12	0	8	7	14
t8P100	15	13	13	11	10	11	9	8	17	13	13	1	9	8	16
t6	13	12	8	9	9	6	7	7	6	11	11	-3	7	7	3
t8	16	13	19	12	11	16	10	8	17	13	13	1	10	8	18
t10	18	15	22	14	12	17	11	10	13	15	15	3	11	10	12
t12	21	15	38	16	14	19	13	11	15	18	15	19	13	11	16
t6R2	8	8	-3	9	9	6	7	7	7	6	7	-14	7	7	3
t6R1	5	5	-7	9	9	6	7	7	6	3	5	-44	7	7	3
t8R2	10	10	2	12	11	17	10	8	17	7	9	-13	10	8	18
t8R1	7	6	6	12	11	17	10	8	18	4	6	-20	10	8	19

Moreover, the component method can predict the maximum resistance of different components. The governing component for one side of the model can be identified, but a single failure mode for the joints cannot be predicted. Therefore, the failure mode of the parametric study is not presented in the paper.

The resistance predicted by the component method is presented in the CM column. For each model, an error in percentage is calculated by  $(\text{CM}/\text{FE}-1) \times 100$ , as presented in the "error" (ERR) column. The deviation of CM prediction varies in a range of -20 % to 13 %. It is worth mentioning that the model t8R1-CCS-CPC with the highest ERR (18 %) is out of the applicable range of the derived component method, as the stiffness difference between the cover plate side and the end plate side is almost three times, leading to bi-axial bending behaviour of the splice. The predicted resistance is 2 % lower than the FE resistance on average. Note that t6RM and t8RM are the simplified models with experimental dimensions and material properties. The comparison of moment-rotation relationships is plotted in Appendix D. The CM curves for the CPT loading condition are offset by a 0.007 radius for an easy comparison between CM and FE results.

### 3.2. Stiffness prediction results

The components, except for components 2), 4), 5), 8), and 9), have either an infinite stiffness or are not relevant for the splice stiffness calculation. The active components for each loading case are listed in Table 5. The stiffness model presented in Table 5 contains three springs (symbol '  $\times$  2' means two springs with the same lever arm), which are the equivalent components based on several individual components. The subscript EP means the equivalent stiffness on the End Plate side, consisting of components 8) and 9). The abbreviation CP stands for Cover Plate side, indicating that the equivalent spring is based on the components 2), 4), and 5). In addition, depending on the position of the equivalent component, a second subscript, "bott" or "side", indicates if the bolt row is at the bottom or on the side of the hollow section.

In general, the same formulas are used for the same type of equivalent components regardless of the "bott" or "side" position. An interesting finding is that the equivalent stiffness of the cover plate in bending on the side wall is different from that under pure tension on the bottom side. Hence, a symbol ' is used in superscript to distinguish two situations,  $k'_{\text{cp,side}}$  and  $k_{\text{cp,bott}}$ . Although the cover plate below the centroid of the column is considered under tension in the resistance calculation, the stiffness of the cover plate in bending cannot be considered in the same way. The reason is that only the bolt furthest from the rotation centre is activated at the elastic stage, indicating that the stiffness model for the cover plate in tension is unsuitable for the cover plate in bending. Fig. 14

depicts a Mises stress contour plot of the cover plate at the end of the elastic stage. It demonstrates that only the furthest bolt contributes to the splice stiffness. In addition, the calculated equivalent stiffness  $k_{\text{cp}}$  based on Components 2), 4), and 5) is in the direction perpendicular to the red dash line between the rotation centre and the bolt centre in Fig. 14. Hence, the projected stiffness  $k'_{\text{cp}}$  is used to represent the stiffness of the cover plate in bending. Besides, all bolts of the cover plate in tension at the bottom of the specimen are activated at the elastic stage, indicating that the activation factor proposed in [10] for asymmetric splice in tension is not required.

The equivalent component on the cover plate side and the end plate side consists of three individual components connected in a row. Hence, Eq. (1) and Eq. (2) are employed to calculate the equivalent stiffness for the cover plate and the end plate, respectively. The equations for each individual component are presented in Appendix C. Fig. 15 shows a flow chart for calculating the joint stiffness.

$$k'_{\text{cp,side}} \text{ or } k_{\text{cp,bott}} = \frac{1}{\frac{1}{k_b} + \frac{1}{k_v} + \frac{1}{k_b}} \quad (1)$$

$$k_{\text{ep,side}} \text{ or } k_{\text{ep,bott}} = \frac{1}{\frac{1}{k_{\text{ep}}} + \frac{1}{k_{\text{bt}}} + \frac{1}{k_{\text{ep}}}} \quad (2)$$

The CM predicted stiffness of experiments and FE models in the parametric study are shown in Table 7. The CM predictions match the FE results well. Note that the predicted stiffness for models with one bolt row in the cover plate might deviate profoundly from FE results, as the equivalent stiffness of the cover plate in bending is very low, leading to a bi-axial bending behaviour. Regardless of models with one bolt row in the cover plate, the maximum, minimum, and average deviations are 38 %, -14 %, and 8 %, respectively.

### 4. Conclusions

The flexural behaviour of two types of asymmetric bolted square hollow section (SHS) splices under five loading conditions is studied through experiments and FE analysis in this paper. The extended component method, validated for asymmetric bolted SHS splices in tension, is verified successfully against the asymmetric splices in bending. Based on the presented results, the following conclusions are drawn.

Twelve components are active in the resistance prediction. Comparing the resistance predicted by the extended component method (CM) to the FE results, the difference varies from -20 % to 13 %, with -2 % on average.

Five stiffness models are proposed for two configurations under

different loading conditions. The extended component method could satisfactorily predict the stiffness of the asymmetric SHS splices. The maximum, minimum, and average deviations of the CM stiffness predictions are 38 %, −14 %, and 8 %, respectively.

The significant difference in stiffness between the two opposite side walls of the splice may lead to an overestimated resistance and stiffness. It is recommended that the stiffness difference should be less than three times.

#### CRediT authorship contribution statement

**Rui Yan:** Writing – review & editing, Writing – original draft, Visualization, Validation, Methodology, Investigation, Formal analysis, Data curation, Conceptualization. **Milan Veljkovic:** Writing – review & editing, Supervision, Resources, Project administration, Methodology, Funding acquisition, Conceptualization. **Luís Simões Da Silva:** Writing – review & editing, Resources, Project administration, Funding acquisition.

#### Declaration of competing interest

The authors declare that they have no known competing financial

interests or personal relationships that could have appeared to influence the work reported in this paper.

#### Data availability

Data will be made available on request.

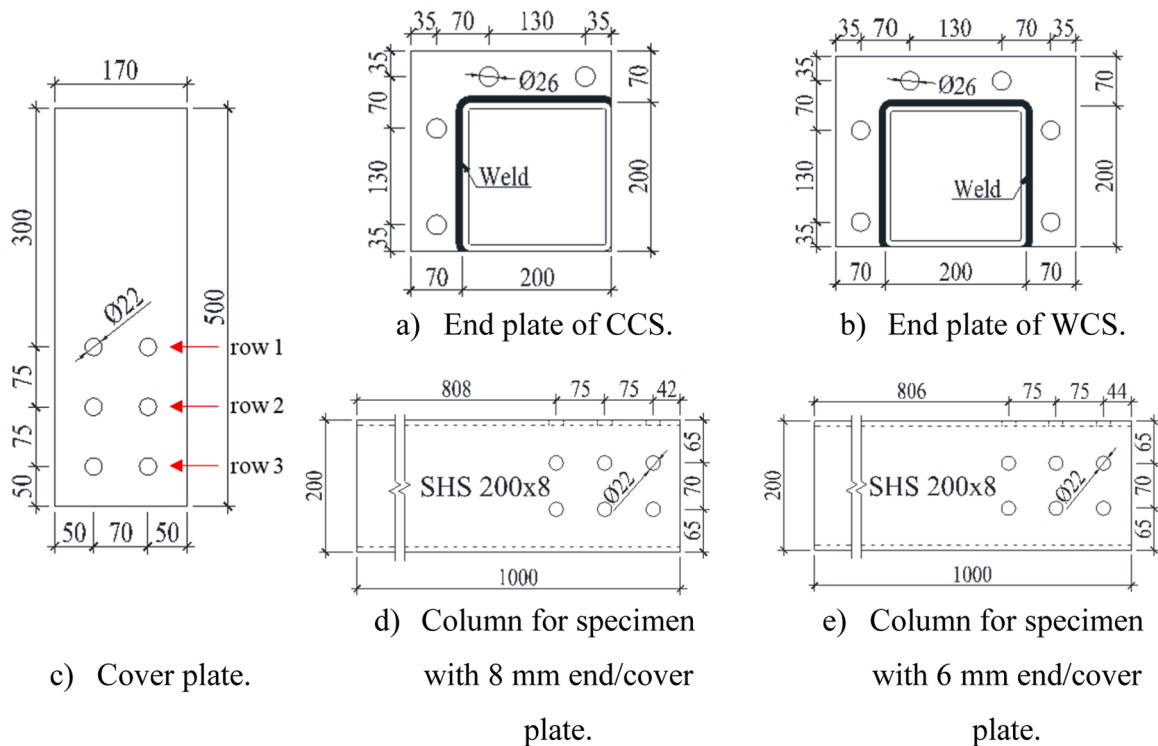
#### Acknowledgments

The research presented in this paper is based on the results of the INNO3DJOINTS project. The work was supported by the RFCS [grant number 749959]. The financial support is thereby gratefully acknowledged.

FCT / MCTES through national funds (PIDDAC) under the R&D Unit Institute for Sustainability and Innovation in Structural Engineering (ISISE), under reference UIDB / 04029/2020, and under the Associate Laboratory Advanced Production and Intelligent Systems (ARISE) under reference LA/P/0112/2020 for the third author.

#### Appendix

##### Appendix A Nominal dimensions of each component [mm] [2]



## Appendix B Design formulas for the resistance of components

- Plate in tension prEN 1993-1-1:2020 [31], Clause 8.2.3

$$N_{t,Rd} = \min\left(\frac{A_g f_y}{\gamma_{M0}}; \frac{A_{net} f_u}{\gamma_{M2}}\right)$$

where  $A_g$  and  $A_{net}$  are the gross area and the net area of the cross-section, respectively.  $f_y$  and  $f_u$  are the yield and ultimate resistance of the plate, respectively.  $\gamma_{M0}$  and  $\gamma_{M2}$  are the partial factors equal to 1.0 and 1.25, respectively.

- Bolts in bearing prEN 1993-1-8:2021 [27], Clause 5.7

$$F_{b,Rd} = \frac{k_m \alpha_b f_u d t}{\gamma_{M2}}$$

$$\text{--for end bolts : } \alpha_b = \min\left(\frac{e_1}{d_0}; 3 \frac{f_{ub}}{f_u}; 3\right)$$

$$\text{--for inner bolts : } \alpha_b = \min\left(\frac{p_1}{d_0} - \frac{1}{2}; 3 \frac{f_{ub}}{f_u}; 3\right)$$

$$k_m = 1 \text{ for steel grade lower than S460, otherwise, } k_m = 0.9$$

where  $f_{ub}$  is the ultimate resistance of the bolt.  $e_1$  is the distance from the bolt centre to the edge of the plate.  $d_0$  is the diameter of the bolt hole.  $p_1$  is the bolt pitch along the loading direction.

- Block tearing failure of the cover plate prEN 1993-1-8:2021 [27], Clause 5.10

$$V_{eff,1,Rd} = \left[ A_{nt} f_u + \min\left(\frac{A_{gv} f_y}{\sqrt{3}}; \frac{A_{nv} f_u}{\sqrt{3}}\right) \right] / \gamma_{M2}$$

where  $A_{nt}$  and  $A_{gv}$  are the net area and the gross area subjected to tension, respectively.

- Bolts in shear prEN 1993-1-8:2021 [27], Clause 5.7

$$F_{v,Rd} = \frac{\alpha_v f_{ub} A_s}{\gamma_{M2}}$$

$$\text{--for property classes 4.6, 5.6 and 8.8 : } \alpha_v = 0.6$$

$$\text{--for property classes 4.8, 5.8, 6.8 and 10.9 : } \alpha_v = 0.5$$

where  $A_s$  is the tensile stress area of the bolt.

- End plate in bending Yan et al. [10]

$$F_{T,1,Rd} = \frac{4M_{pl,1,Rd}}{m}$$

$$M_{pl,1,Rd} = 0.25 \sum l_{eff,1} t^2 f_y / \gamma_{M0}$$

where  $\sum l_{eff,1}$  is the effective length of the equivalent T-stub,  $f_y$  is the yield strength of the material.

For Corner T-stub:



$$l_{\text{eff,cor}} = am + bn + ce^* \quad l_{\text{eff,para}} = \min \left\{ \left[ f \left( e^* / \frac{p}{2} \right) + g \right] m, p \right\}$$

$$a = -0.69 \frac{d}{t} + 1.86 \quad f = -1.33$$

$$b = 1.61 \frac{d}{t} - 2.64 \quad g = 0.95 \frac{d}{t} + 2.00$$

$$c = 1.42$$

For Edge T-stub:

$$l_{\text{eff,edge}} = am + bn + ce^* \quad l_{\text{eff,para}} = \min \left\{ \left[ f \left( e^* / \frac{p}{2} \right) + g \right] m, p \right\}$$

$$a = -0.26 \frac{d}{t} + 0.50 \quad f = -1.64$$

$$b = 1.16 \frac{d}{t} - 2.65 \quad g = 1.20 \frac{d}{t} + 2.03$$

$$c = 1.97$$

where  $n$  is  $\min(1.25 m, e)$ ;  $d$  is the diameter of the bolt;  $a$ ,  $b$ ,  $c$ ,  $f$ , and  $g$  are coefficients; the rest of the dimensions are visible in Fig. 12.

For Corner T-stub:

- Bolts in tension prEN 1993-1-8:2021 [27], Clause 5.7

$$F_{t,Rd} = \frac{0.9 f_{ub} A_s}{\gamma_{M2}}$$

- Column flange and web in compression prEN 1993-1-8:2021 [27], Clause A.10

$$F_{c,fb,Rd} = \frac{M_{c,Rd}}{h - t_{fb}}$$

where  $M_{c,Rd}$ ,  $h$ , and  $t_{fb}$  are the design moment resistance of the cross-section, depth of the column, and the thickness of the tube, respectively.

#### Appendix C Design formulas for the stiffness of employed components

- Bolts in bearing prEN 1993-1-8:2021 [27], Clause A.15.2

$$k_b = \frac{\bar{S}_b n t_j f_u}{E} \quad \bar{\sigma}_{b,Ed} = \frac{F_{v,Ed}}{d t_j f_u}$$

$$\bar{S}_b = \frac{\bar{\sigma}_{b,Ed}}{\frac{u}{d} (\bar{\sigma}_b = \bar{\sigma}_{b,Ed})} \quad \bar{\sigma}_b = \frac{126u/d}{(1 + \sqrt{30u/d})^2}$$

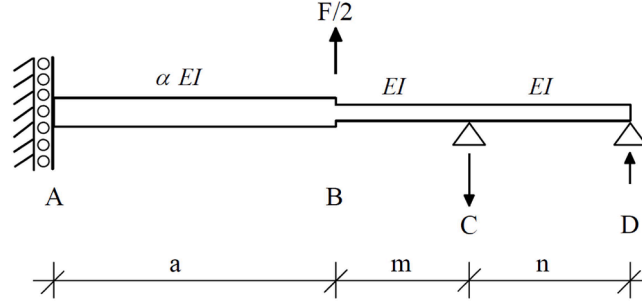
where  $n$  is the number of bolts;  $f_u$  is the ultimate tensile strength of the steel plate to which the bolt bears;  $t_j$  is the thickness of the plate component;  $\bar{S}_b$  is the relative bearing stiffness;  $\bar{\sigma}_{b,Ed}$  is the non-dimensional average bearing stress;  $u/d (\bar{\sigma}_b = \bar{\sigma}_{b,Ed})$  is the non-dimensional bolt hole elongation at non-dimensional design bearing stress;  $u$  is the bolt hole elongation;  $d$  is the bolt diameter;  $\bar{\sigma}_b$  is the non-dimensional average bearing stress;  $F_{v,Ed}$  is the design shear force per bolt which equals to the design resistance on the cover plate side divided by the number of bolts.

- Bolts in shear prEN 1993-1-8:2021 [27], Clause A.14.2

$$k_v = \frac{16 n_b d^2 f_{ub}}{E d_{M16}}$$

where  $d_{M16}$  is the nominal diameter of an M16 bolt and  $n_b$  is the number of bolt rows (with two bolts per row).

- End plate in bending Karlsen and Aalberg [26] and Yan et al. [10]



$$k_{ep} = \frac{2(3a + 3m\alpha + n\alpha) \cdot l_{eff,ini} \cdot t_p^3}{m^2(3m^2\alpha + 4nma + 12am + 12an)}$$

$$l_{eff,ini} = R \times l_{eff}$$

$$R = h \frac{m}{\sqrt{m^2 + e^{*2}}} + j$$

where  $a$  is the distance from the sidewall of the tube to the symmetry line inside the tube;  $\alpha$  reflects the 2D bending effect, which increases the stiffness of the end plate inside the tube;  $l_{eff,ini}$  is a modified effective length. The parameters  $a$  and  $\alpha$  are 100 mm and 1 in the studied cases, respectively.

For Corner T-stub:

$$h = 0.21 \frac{d}{t} + 0.24$$

$$j = 0.26 \frac{d}{t} - 0.36$$

For Edge T-stub:

$$h = 0.81$$

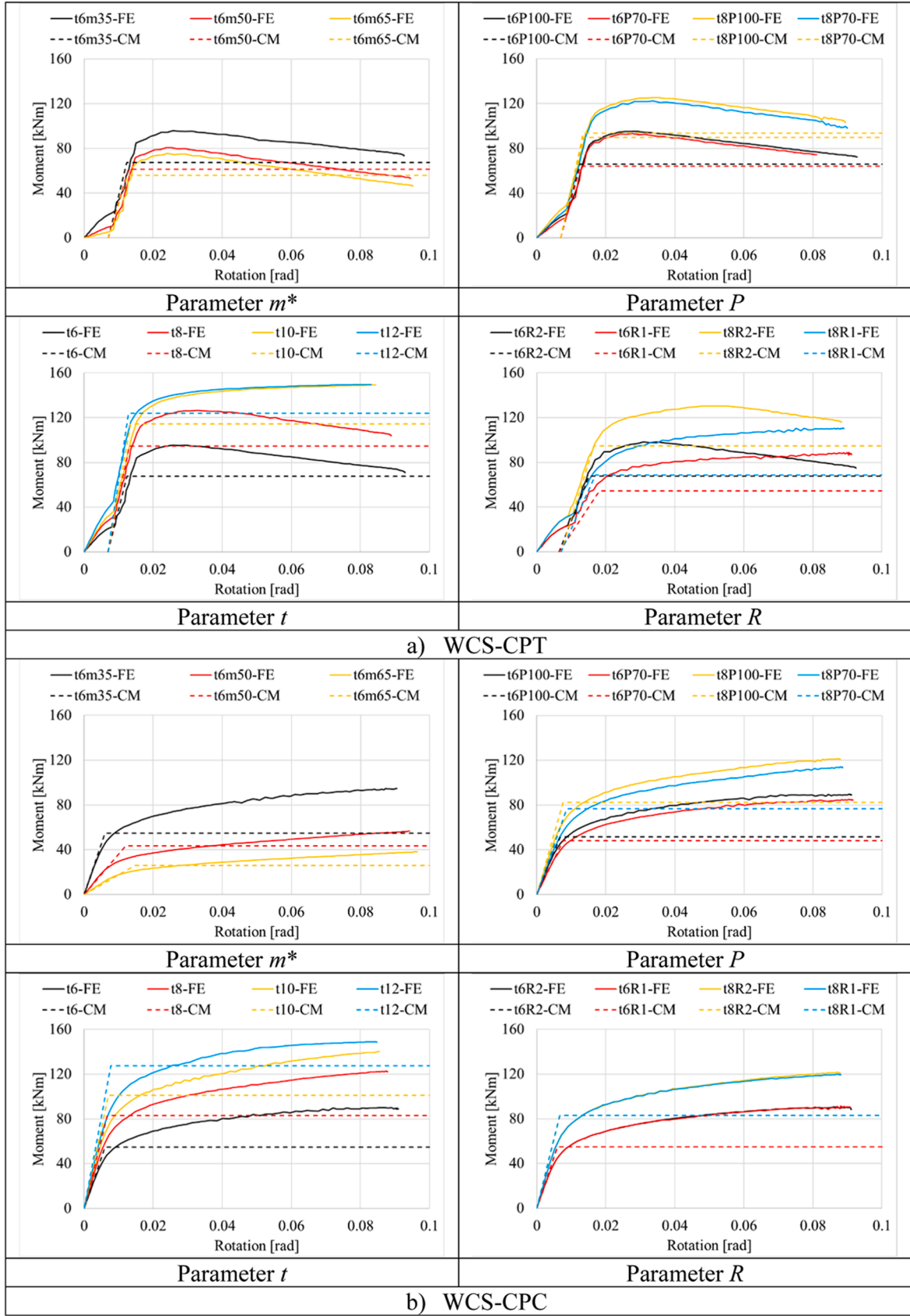
$$j = 0.36 \frac{d}{t} - 0.62$$

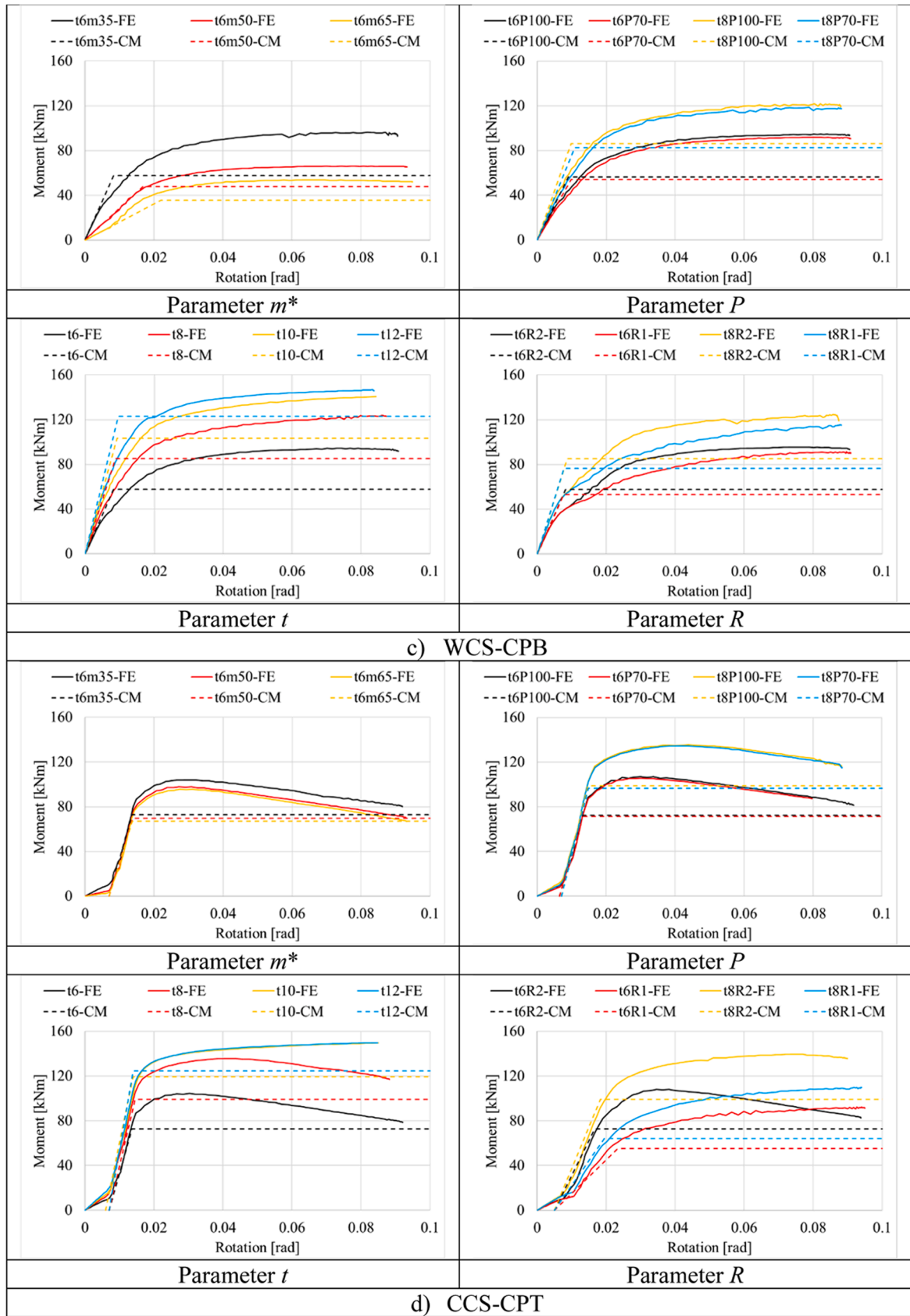
- Bolts in tension Karlsen and Aalberg [26]

$$k_{bt} = \frac{4n(3a + 3m\alpha + n\alpha)}{(6am + 6an + 3m^2\alpha + 2n^2\alpha + 6nma)} \frac{A_b}{L_b}$$

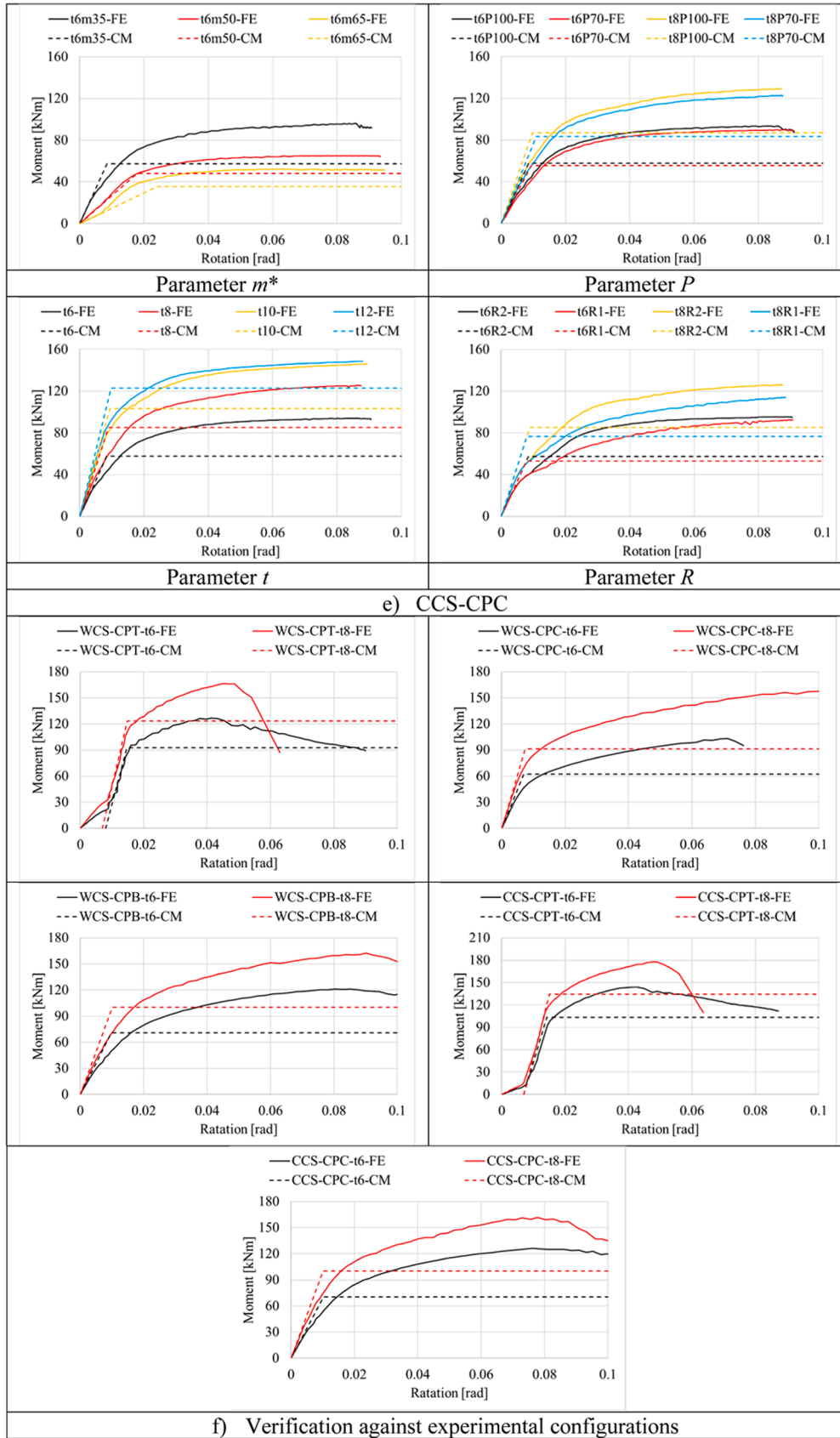
where  $L_b$  is the bolt elongation length.

Appendix D Moment-rotation relationships









## References

- [1] C.V. Miculaş, R.J. Costa, L. Simões Da Silva, R. Simões, H. Craveiro, T. Tankova, 3D macro-element for innovative plug-and-play joints, *J. Constr. Steel Res.* 214 (2024) 108436, <https://doi.org/10.1016/j.jcsr.2023.108436>.
- [2] R. Yan, H. Xin, M. Veljkovic, L.S. da Silva, Tensile behaviour of asymmetric bolted square hollow section column splices, *Thin-Wall. Struct.* 190 (2023) 111014, <https://doi.org/10.1016/j.tws.2023.111014>.
- [3] T. Tankova, H. Craveiro, C. Silva, F.F. Ribeiro, R. Simões, C. Martins, R. Costa, L. Simões Da Silva, Behaviour of plug-and-play joints between RHS columns and CFS trusses, *Structures* 41 (2022) 1719–1745, <https://doi.org/10.1016/j.istruc.2022.05.099>.
- [4] L. Cheng, F. Yang, M. Seidel, M. Veljkovic, FE-assisted investigation for mechanical behaviour of connections in offshore wind turbine towers, (2023). <https://doi.org/10.1016/j.engstruct.2023.116039>.
- [5] L. Cheng, F. Yang, J.S. Winkes, M. Veljkovic, The C1 wedge connection in towers for wind turbine structures, tensile behaviour of a segment test, (2023). <https://doi.org/10.1016/j.engstruct.2023.115799>.
- [6] X.-M. Lin, M.C.H. Yam, K.-F. Chung, A.C.C. Lam, A study of net-section resistance of high strength steel bolted connections, (2020). <https://doi.org/10.1016/j.tws.2020.107284>.
- [7] X.-M. Lin, M.C.H. Yam, Y. Song, K.-F. Chung, H.-C. Ho, Y. Han, Net section tension capacity of high strength steel single shear bolted connections, *Thin-Wall. Struct.* 195 (2024) 111371, <https://doi.org/10.1016/j.tws.2023.111371>.
- [8] C. Wang, R. Tremblay, C.A. Rogers, Component-based model for bolted brace connections in conventional concentrically braced frames, (2021). <https://doi.org/10.1016/j.engstruct.2021.113137>.
- [9] C. Wang, R. Tremblay, C.A. Rogers, Parametric study on the I-shape brace connection of conventional concentrically braced frames, (2021). <https://doi.org/10.1016/j.jcsr.2021.106669>.
- [10] R. Yan, M. Veljkovic, Component method for bolted SHS end plate splice joints loaded in tension, *Structures* 59 (2024) 105704, <https://doi.org/10.1016/j.istruc.2023.105704>.
- [11] F. Yang, Y. Liu, Z. Jiang, H. Xin, Shear performance of a novel demountable steel-concrete bolted connector under static push-out tests, (2018). <https://doi.org/10.1016/j.engstruct.2018.01.005>.
- [12] F. Yang, Y. Liu, H. Xin, M. Veljkovic, Fracture simulation of a demountable steel-concrete bolted connector in push-out tests, (2021). <https://doi.org/10.1016/j.engstruct.2021.112305>.
- [13] G.Q. Li, K. Liu, Y.B. Wang, Z. Dai, Moment resistance of blind-bolted SHS column splice joint subjected to eccentric compression, *Thin-Wall. Struct.* 141 (2019) 184–193, <https://doi.org/10.1016/j.tws.2019.04.015>.
- [14] M. Mahmood, W. Tizani, A component model for column face in bending of extended HoloBolt connections, *J. Constr. Steel Res.* 182 (2021) 106655, <https://doi.org/10.1016/j.jcsr.2021.106655>.
- [15] P. Wang, L. Sun, B. Zhang, X. Yang, F. Liu, Z. Han, Experimental studies on T-stub to hollow section column connection bolted by T-head square-neck one-side bolts under tension, *J. Constr. Steel Res.* 178 (2021) 106493, <https://doi.org/10.1016/j.jcsr.2020.106493>.
- [16] R. He, X. Shu, Z. Zhang, Experimental study on the tensile performance of high-strength blind-bolted T-stub with endplate tapping, *J. Eng. Sci. Technol. Rev.* 11 (2018) 109–118, <https://doi.org/10.25103/jestr.115.13>.
- [17] M. D'Antimo, J.F. Demonceau, J.P. Jaspart, M. Latour, G. Rizzano, Experimental and theoretical analysis of shear bolted connections for tubular structures, *J. Constr. Steel Res.* 138 (2017) 264–282, <https://doi.org/10.1016/j.jcsr.2017.07.015>.
- [18] L. Roquete, M.M. de Oliveira, A.M.C. Sarmanho, E.M. Xavier, V.N. Alves, Behavior and design formulation of steel CHS with sleeve connections, *J. Constr. Steel Res.* 177 (2021) 106465, <https://doi.org/10.1016/j.jcsr.2020.106465>.
- [19] Z. Chen, J. Liu, Y. Yu, Experimental study on interior connections in modular steel buildings, *Eng. Struct.* 147 (2017) 625–638, <https://doi.org/10.1016/j.engstruct.2017.06.002>.
- [20] S.N. Sadeghi, A. Heidarpour, X.L. Zhao, R. Al-Mahaidi, A component-based model for innovative prefabricated beam-to-hybrid tubular column connections, *Thin-Wall. Struct.* 132 (2018) 265–275, <https://doi.org/10.1016/j.tws.2018.08.021>.
- [21] B. Kato, A. Mukai, Bolted tension flanges joining square hollow section members, *J. Constr. Steel Res.* 5 (1985) 163–177, [https://doi.org/10.1016/0143-974X\(85\)90001-X](https://doi.org/10.1016/0143-974X(85)90001-X).
- [22] J.A. Packer, L. Bruno, P.C. Birkmoe, Limit analysis of bolted RHS flange plate joints, *J. Struct. Eng.* 115 (1989) 2226–2242, [https://doi.org/10.1061/\(asce\)0733-9445\(1989\)115:9\(2226\)](https://doi.org/10.1061/(asce)0733-9445(1989)115:9(2226)).
- [23] Y. Steige, K. Weynand, Design resistance of end plate splices with hollow sections, *Steel Construct.* 8 (2015) 187–193, <https://doi.org/10.1002/stco.201510023>.
- [24] S. Willibald, Bolted Connections for Rectangular Hollow Sections under Tensile Loading, Karlsruhe Institute of Technology, 2003, <https://doi.org/10.5445/IR/1672003>.
- [25] M. Heinisuo, H. Ronni, H. Perttola, A. Aalto, T. Tiainen, End and base plate joints with corner bolts for rectangular tubular member, *J. Constr. Steel Res.* 75 (2012) 85–92, <https://doi.org/10.1016/j.jcsr.2012.03.013>.
- [26] F.T. Karlsen, A. Aalberg, Bolted RHS End-Plate Joints in Axial Tension, in: *Nordic Steel Construction Conference*, Oslo, 2012. <http://hdl.handle.net/11250/228203>.
- [27] CEN, prEN 1993-1-8:2021 - Design of steel structures - Part 1-8: design of joints (draft of EN1993-1-8: 2021), (2022).
- [28] S. Swierczyna, Study on bolted and blind-bolted single shear connections of cold-formed steel members, *Archit. Civil Eng. Environ.* (2020), <https://doi.org/10.21307/ACEE-2020-023>.
- [29] Blind bolt without sleeve, (n.d.). <https://www.blindbolt.co.uk/the-blind-bolt/>.
- [30] ABAQUS, Abaqus Analysis User's Manual, 6.14 version, (2014).
- [31] CEN, prEN 1993-1-1:2020 - Design of steel structures - Part 1-1: general rules and rules for buildings (draft of EN1993-1-1: 2020), (2021).